

CHARACTERISTICS OF DISPLAY SYSTEMS IN SCANNING AND A SIMPLE PHANTOM PROCEDURE TO EVALUATE OVER-ALL SCANNER PERFORMANCE

J. R. Mallard and R. J. Wilks

Department of Medical Physics, University of Aberdeen, Aberdeen, Scotland

A description of the performance of a radioisotope scanning machine invariably involves the concepts of "sensitivity" and "resolution." Both terms have been defined in different ways by several authors, either to give a more adequate performance description of a scanner for a particular purpose or to illustrate more clearly the properties of a particular type of scanner.

The contending terms for sensitivity include the concept of "point-source" and "extended-source" efficiencies; for resolution, the width of the 50% or 10% (or lower) isocount contour as well as the separation of two point sources which can be just distinguished have all been used. The continuing multiplicity of different types of scanning machines, both of the moving-detector (conventional) and the stationary-detector (camera) type, is accentuating the need for universally acceptable definitions (1,2).

In addition, for any one machine, the use of different isotopes, different collimators, different operating conditions and different display settings for a given clinical scanning situation offer a wide range of sensitivity and resolution values. Since the two terms are closely interdependent, there is a need for an over-all performance concept containing in some way both sensitivity and resolution to describe the suitability of a particular arrangement for the problem to be tackled.

One method of providing an over-all performance index is the "figure of merit" (3-5). In this approach, the counting-rate rise given by the particular detector when it views a certain radioisotope distribution is calculated or determined experimentally. Its weakness in our opinion lies in the assumption that this counting-rate rise will be displayed by the display system and seen by the eye if the counting-rate change exceeds (usually) three standard deviations of the background counting rate in the surrounding regions. This change of counting rate is regarded as that which is statistically significant.

However, a poor display system may not be capable of demonstrating this particular change of counting rate, or, alternatively, it may be able to demonstrate much smaller changes of counting rate which therefore might *not* be statistically significant. In short, the "figure of merit" does not take into account the visualizing properties of the display; it only sets a fairly arbitrary threshold of statistical significance. We believe that the approach described here takes into account both the visual and the statistical significance aspects of the display. The relationship between the method proposed here and the "figure of merit" is discussed in more detail later.

Finally, although the "figure of merit" is of value for intercomparing counter-collimator systems, we felt that a comparison that was rather more meaningful in clinical terms was needed.

At the moment, scanning is used almost entirely to detect regions of abnormally increased or decreased counting rate in a general pattern of radioactivity with a distribution that can be recognized as "normal." While it is likely that in the future it may be possible to show, for example, blood vessels with an abnormal pattern or distribution which could be regarded as being "line sources," the present-day use for scanning is essentially for detection of "area sources" with either increased or decreased radioactive concentration relative to the surroundings. We therefore set out to devise a procedure which could be used to determine the minimum size of "area-source" made perceptible by the scanning machine in *any* set of scanning conditions. We have used circular areas, but there is no reason why any other shape cannot be used including, in the limit, line sources.

Basically, the procedure, which is described in detail later, is simple. It consists of determining the counting-rate change detected by the counter from

Received Oct. 10, 1966; revision accepted May 18, 1967.

a sectional cylindrical source in a "body-background" tank. From a comparatively small number of measurements it is possible to evaluate the counting-rate change for a very wide range of circumstances. It is then necessary to know whether the calculated counting-rate change is made visible to the eye by the display. Here we were unable to find much information in the literature, so we decided to carry out a supplementary experiment to determine the characteristics of several different display systems used in practice. These experiments and their results are described in the next section. It should be stressed here that these experiments were performed not only to learn more about display systems and their subjective mode of action on the eye and brain, but primarily to obtain results that are used in the phantom procedure for scanner-performance evaluation.

While this work was in progress, Beck (6) proposed the use of the "modulation transfer function" as a measure of scanner performance. This technique is undoubtedly of great value even though the concept and its use requires further development. The phantom technique described here may be regarded as complementary to it, and the relationship between them is discussed later in this paper.

DISPLAY CHARACTERISTICS

The following are the more common of the radioisotope scanning displays used in practice:

Moving-detector systems:

1. Black marks printed on white paper.
2. Colored marks printed on white paper.
3. Monochrome photographic recording.
4. Colored photographic recording.
5. Profile chart recording from a ratemeter.
6. Digital displays—usually used in conjunction with some other pictorial display.

Stationary-detector systems:

7. Picture usually stored on a photograph either from a cathode-ray tube (or phosphor of an image intensifier) for a gamma camera or directly photographed in the case of a spark chamber.

8. Two-dimensional digital printout obtained with a multichannel analyzer or other computer system.

Although this paper considers particular examples of displays 1, 2, 3 and 7 only, the technique is applicable to the others. The experimental method is described for one display—a color printing display (7)—and the results are presented for the others.

Color display. Hollow disks 1-cm thick with diameters of 1, 2, 3 and 4 cm were filled with known amounts of the radionuclide under consideration and were scanned in a tissue-equivalent phantom of MIX-D wax by the particular counting system being used for scanning with that isotope; the background

counting-rate was provided by a small active source attached to the lead shielding of the counter. A series of scans was performed, and the background counting-rate was varied by adjusting the position of this source relative to the counter over a range of 5–100 cps while the counting rate over the disks was varied in steps by replacing one disk with another of the same dimensions containing a different amount of activity. In each scan the background counting rate was chosen in advance in such a way that, as nearly as possible, the appropriate increase of counting rate due to a given disk at a given position was just detected by visual examination of the display. About five scans were carried out at different background counting rates for each disk. The scanning speed was 0.2 cm/sec and the printout factor was chosen to give a mark at least every 2 or 3 mm. In this way, the marks/unit area was kept constant (of the same order as, say, a brain scan) and for the range of background counting rates examined the count density varied from 50 to 1,000 counts/cm².

Sixty-nine color scans were performed, and six people examined each scan visually and estimated which scan in each series gave the visual threshold of detectability. Two of these people were not skilled in scan interpretation. The average of their estimations is shown in graphical form in Fig. 1A and B. Figure 1A shows a typical plot of the threshold incremental counting rate n_{Th} necessary for visual perception as a function of the background counting rate N for the sizes of disks and depths in the phantom. For $5 \leq N \leq 100$ cps the relationship approximates a straight line of slope 0.10. Figure 1B summarizes the results for all disks in all positions. The errors shown are measures of the spread of the slopes calculated from graphs similar to Fig. 1A.

Taking the errors into account, it appears that the threshold incremental counting rate n_{Th} due to any disk of any size from 1 to 4 cm diameter at any depth from 0 to 10 cm which the color display can just render perceptible to the eye is proportional to the total background counting rate N such that $n_{Th}/N = 0.10 \pm 0.01$. Thus a 10% increase of counting rate above background at the center of the disk scan is just detected.

This figure is in good agreement with that derived from statistical considerations (8) for the same display system. Other color printing displays may use a different color-coding system, but it is thought unlikely that there will be significant differences in their display detectabilities since this is essentially a color-boundary process at the limit of detection.

Black and white mark displays. A very preliminary analysis of displays using black marks on white paper was performed by taking carbon copies of the scans

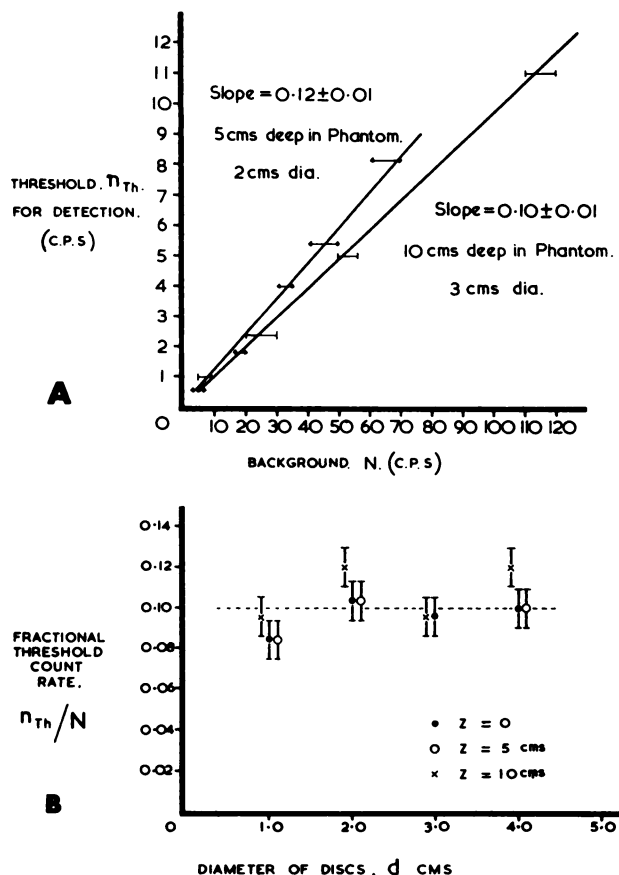


FIG. 1. Thresholds for color display. In A, range of estimates of six people viewing series of scans for two examples plotted show linear relationship between threshold increase in counting rate for visual perception and background counting rate. In B, graph is plotted for all sizes, depths and backgrounds used. Ordinates are gradients of lines similar to two examples in A. 10% increase of counting rate is required for threshold of visual perception which appears to be largely independent of parameters examined.

above. Since the visual interpretation of such scans is not aided by color, the n_{Th} was found to be correspondingly higher, and for the scans which were at the threshold value, typical values of n_{Th}/N were 0.20 or more. This figure probably varies with N. It was not necessary to perform any detailed analysis of these displays because, as purely visual displays, they have been superseded very largely by either color displays or photographic displays which, although the latter are *visually* superior, present the same digital information.

Photographic display. A more thorough analysis was carried out for a photographic display (Picker Magnascanner) using the 19-hole collimator and counter supplied. However, in this case an analysis was not made with depth in the phantom as it was in the color display. Instead we chose a depth of 5 cm because we were primarily interested in a direct comparison between color and photographic displays. Thirty-five scans were performed, and Fig. 2 shows

the plot of n_{Th}/N for different diameters of disks. Rather surprisingly, the ordinate is very close to 0.10, the same value as for the color printing display, when a density setting of "25" or "50" on the Magnascanner control panel is used. The setting of "100" was not considered to give the best scans, and so was not included in the analysis.

An interesting observation which has arisen from the scans is that the photographic density changes required for the visual detection of the disks was at least 50%; values for four cases were 50%, 100%, 100% and 165%. This was measured by taking an average value of density over the disk region and comparing this to an average value over the background. Thus a 10% increase in counting rate yields at least a 50% increase in film density for the settings of the Picker Magnascanner described above.

Laughlin (9) quotes a much lower figure of 10% for the change in photographic density needed for visual detection, but we believe that he has measured this in a somewhat different way. If we understand his method correctly, he scanned disks and altered the photographic density using the display controls of the scanning machine. This process was carried out for several disk sizes, and an estimate of the minimum density change which could be distinguished from disk to disk was made. Our measurements involve scanning and perceiving a disk in a background "sea" of counting rate and incorporate the effects due to counting statistics to a greater extent. Therefore although a 10% variation of photographic density can still be visually distinguished in our case for *very small areas*, the *average change*

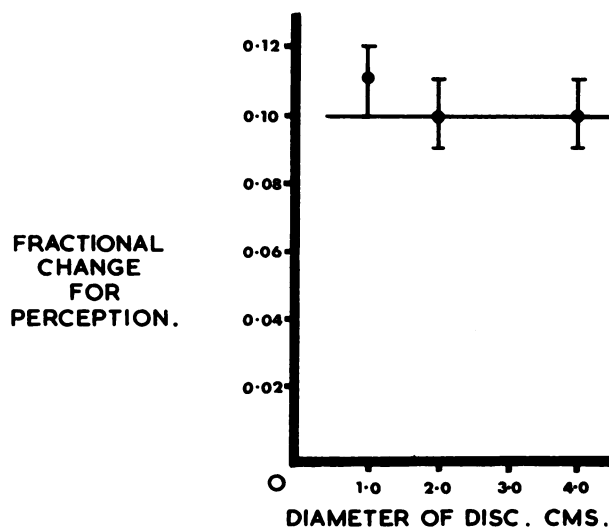
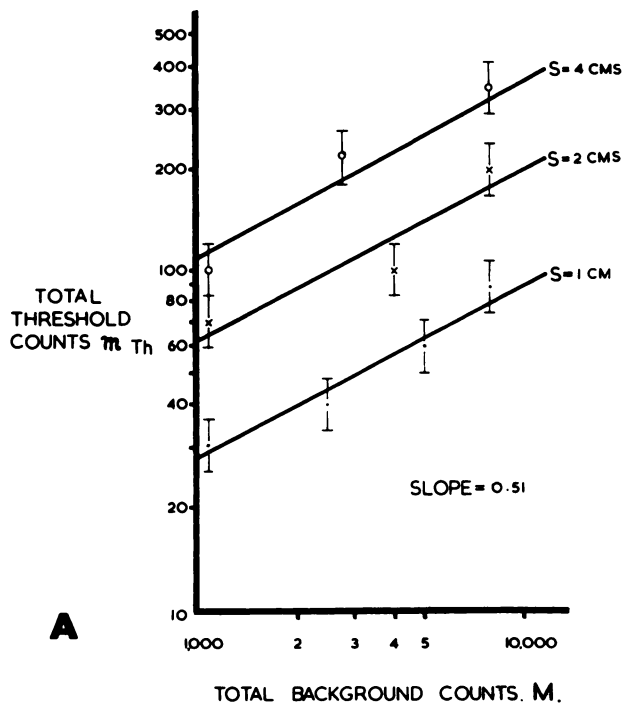
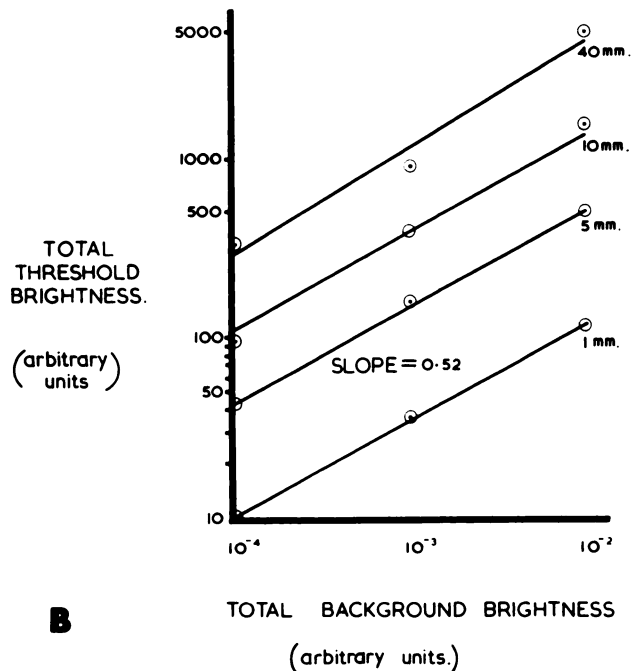


FIG. 2. Characteristics of photographic display analogous to Fig. 1B using Picker Magnascanner display. Only one depth of 5 cm was used. Again threshold is 10% within experimental error for condition examined.

THRESHOLD COUNTS vs BACKGROUND COUNTS
FOR DIFFERENT DIAMETER OF THRESHOLD COUNTS. S.



EXTRAPOLATION OF MORGAN'S RESULTS FOR
VISUAL THRESHOLDS OF BRIGHT DISCS IN
BACKGROUND LEVELS OF ILLUMINATION



required for perception of the disk over an area of the same order as the disk is increased by the statistical density changes that occur.

Storage cathode-ray-tube displays. Storage cathode-ray-tube displays and conventional cathode-ray tubes are used with gamma cameras. For ease and convenience in our display experiments, we used a pinhole gamma camera with a point source, but there is no reason why a multichannel parallel-hole collimator and sources of different diameters could not be used instead.

The point source was placed at the pinhole, and the uniform picture that resulted was allowed to integrate on the 10-cm-diameter storage-tube display until a measured number of scintillations M (and therefore displayed dots) had accumulated. The source was then lowered beneath the pinhole to a predetermined position so that a known area of the cathode-ray tube accumulated counts. The display was again switched on until the area of increased dot density was just visible to the eye and the extra number of dots, m_{Th} , were recorded. Photographs were taken, and the experiment was repeated for different numbers of dots in the uniform background and for different areas of increased dot density. Thirty-four photographs were made altogether with care taken to ensure that the photographic record was as closely as possible visually identical with the displayed image.

FIG. 3. Threshold of cathode-ray-tube display used with gamma camera. In A, total counts required to perceive disk (of displayed diameter s) is plotted against total background counts over whole display. The relationship is seen to be $m_{Th} \propto M^{1/2}$. B shows results of Morgan (10) for the visual thresholds of bright disks on photographic film in three different background levels of illumination. His published values have been replotted here in arbitrary units of total light flux to compare them directly with those in A. Result is again square-root relationship.

Although a few measurements were taken with some degree of contrast enhancement, the results reported here only apply to the untreated pictures. Contrast enhancement was very effective at the higher dot densities, probably because the storage mesh became saturated at high values of dot densities; i.e., further charge deposits on the storage mesh no longer resulted in a corresponding increase of display brilliance because the whole brilliance of the flood gun was being used at that region already. The adjustment of the backing-electrode potential, which provides contrast enhancement, normalized the maximum brilliance to the maximum transmission of the flood gun, restoring linearity and therefore contrast.

Different settings of individual dot brightness could, of course, be used to optimize visual detection for a given background dot density, but it was thought better to use a typical setting and retain this throughout.

The results obtained for the storage tube will be the same as for a conventional cathode-ray tube,

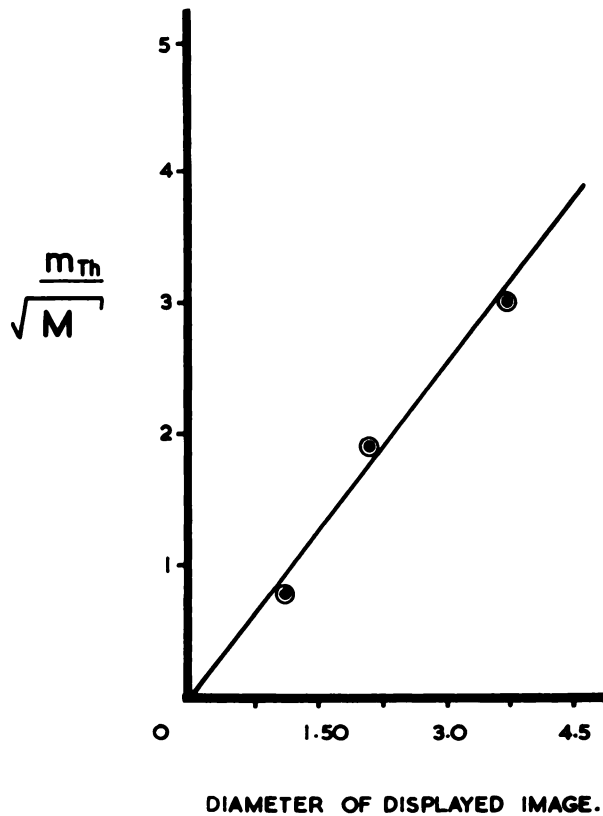


FIG. 4. Threshold of cathode-ray-tube display used with gamma camera. Points of graph are obtained directly from Fig. 3A and show that threshold is proportional to size, s , for given value of background total counts.

provided these saturation effects are kept to a minimum. They can, in fact, be completely eliminated by using the storage tube as a normal cathode-ray tube, but this increases the number of photographs required for the threshold experiment and is generally more time consuming.

When m_{Th} was plotted as a function of M for a given disk size on log-log paper (Fig. 3A), straight lines of slope 0.5 resulted within the experimental error. This indicated that $m_{Th} \propto M^{1/2}$ for a given disk size.

After this experimental work was completed, our attention was drawn to the results of Morgan (10) working in the rather different field of radiographic perception, and this has led to a most interesting comparison. He investigated the threshold contrast of bright disks ranging in diameter from 0.3 to 100 mm in three different levels of background illumination. Although the visual perception of such films depends on factors such as viewing distance, degree of focus of the image and the eye "line of sight," the typical curves shown in Fig. 2 of his paper are used here for comparison.

Morgan's pictures are composed of a large number of small dots, each of photographic grain size

with individual low light intensity, whereas our pictures are the reverse of this, i.e., they show a comparatively small number of bright diffuse dots. Therefore, the *average* brightness per unit area of the two types of pictures is given by the product of the number of dots per unit area and the brightness of each dot; the relative statistical variation of this figure is considerably greater in our case for the same value of average brightness. However, replotting Morgan's curves in terms of total light flux (i.e., brightness multiplied by the area of the disk, which compares directly with m), Fig. 3B resulted. Again, this shows straight lines with a slope approximately equal to 0.52 so that agreement with the square-root law found in our experiment is good; the agreement is the more interesting in view of the rather different experimental conditions involved. For example, the profile of counts across the displayed image for the cathode-ray-tube experiment was bell shaped, whereas the profiles of brightness across the disks in Morgan's experiment were square shaped. Also as mentioned before, statistical effects were of more importance in our experiment. However, within the experimental error, the statistics do not seem to have altered the basic square-root law.

Returning to our original experiment, we found (Fig. 4) that

$$m_{Th}/M^{1/2} = ks \quad (1)$$

where s is the diameter of the displayed image and k is approximately 0.80.

The equivalent of this graph extrapolated from Morgan's curves resulted in a reasonably straight-line graph out to a diameter of 1 cm after which the slope increased with increasing diameter. However, bearing in mind the errors involved in extrapolating from a small published graph and the somewhat greater errors involved in the cathode-ray-tube experiment, the straight-line relationship up to values of $s = 4$ cm is considered to be very reasonable.

To effect a direct comparison between the cathode-ray-tube display now under consideration and the other displays investigated here, it was required to measure the height of both the background H and the profile incremental counts h due to cylindrical disks in phantom (as described earlier) using either a pinhole or multichannel collimator with the gamma camera under the same phantom conditions.

The terms h and H were measured experimentally using a multichannel analyzer (Laben 512 A 51 CISE) operating in the x-y mode (11) and set so that the elementary area was much less than the width of the profile so that a true estimation of profile height could be obtained. For the profiles we encountered with the multichannel collimator (Fig.

5A) the volume m for a given height of profile h was found in practice to be proportional to s (Fig. 5B) giving rise to the following relationship

$$m = chs \tag{2}$$

where $c \doteq 8.2$ for $s \geq 1.0$ cm. This unexpected relationship holds up to $s = 4$ cm because of the poor total resolution of the gamma camera which results in the profiles not being flat-topped for sources up to about 4 cm diameter as shown in Fig. 5A. In fact, the height of the profile is approximately proportional to the disk diameter (Fig. 5C) instead of remaining constant for different diameters of sources containing the same concentration of isotope. The equivalent of Morgan's "square" profiles, however, will remain of constant height.

Figure 5C also shows as a dotted line the results obtained in exactly the same manner using a pinhole. The fact that both curves agree so closely indicates the similarity of the profile shapes presented to the display with both multichannel and pinhole collimators. Hence, as far as this work is concerned, the

pinhole and collimator profile characteristics are interchangeable.

Now, $m \propto$ total activity in the disk $\propto d^2$ and $h \propto d$ (Fig. 5C) where d is the diameter of the disk source. Therefore $m/h \propto d$, and d is approximately proportional to s for $d \geq 1.5$ cm; i.e., when d is greater than the total resolution of the system. Thus we have $m \propto hs$, which is found in practice (Eq. 2).

Substituting Eq. 2 in Eq. 1 together with $M = 200 H$ (i.e., the whole of the background being contained in 200 channels of the multichannel analyzer) then

$$sh_{Th}/H^{1/2} = s(200)^{1/2} 0.80/8.2 \tag{3}$$

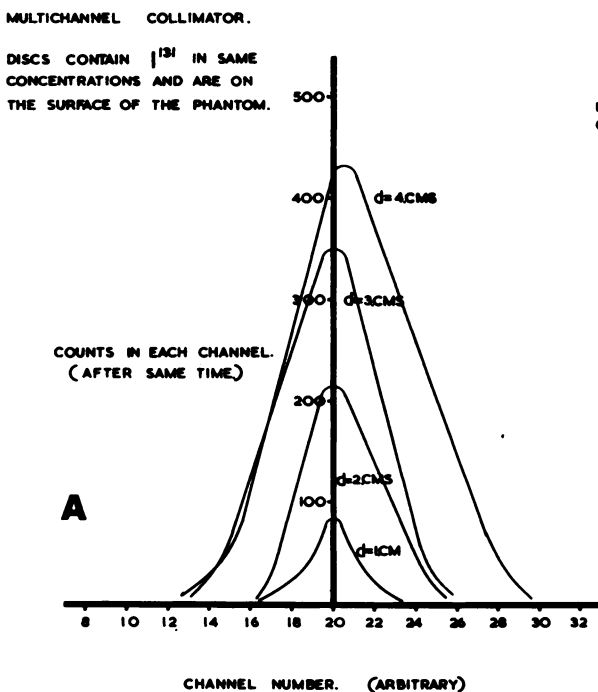
i.e.,

$$h_{Th}/H^{1/2} = 1.40 \pm 0.05$$

and is independent of s for $s > 1.0$ cm.

For $s \leq 1.0$ cm the linearity of Fig. 5B is not maintained, as is shown by the dotted line on the graph. This results in the value of $h_{Th}/H^{1/2}$ gradually increasing with diminishing s , i.e., a greater profile height is needed for threshold detection. However, for $1.0 \leq s \leq 4.0$ cm, which covers the range found in most clinical cases, Eq. 3 can be used.

PROFILE ACROSS A DIAMETER OF THE DISPLAY.



VOLUME OF COUNTS vs DIAMETER OF DISPLAY FOR GIVEN HEIGHT OF PROFILE.

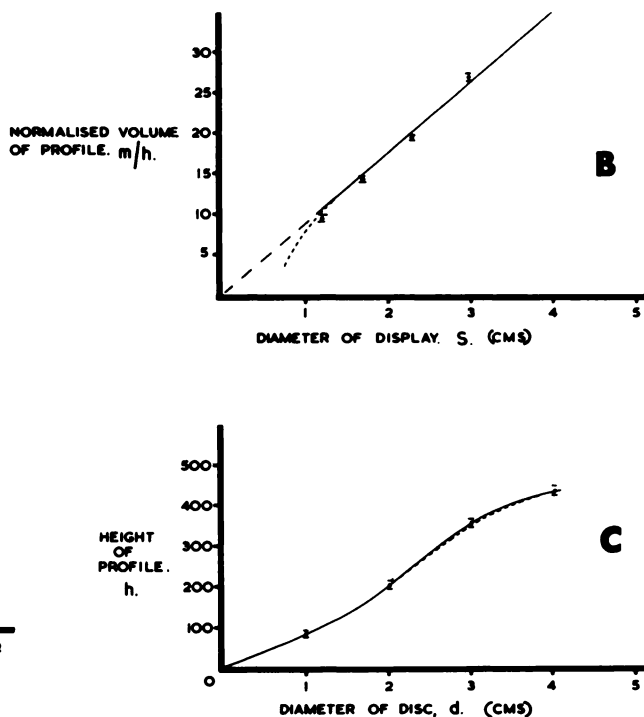
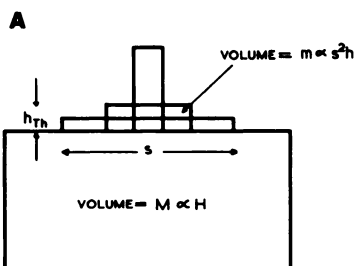


FIG. 5. Some characteristics of profiles presented to cathode-ray-tube display. A shows typical profiles of counting-rate information presented by image-transfer system of gamma camera to its display system. These were measured with multichannel analyzer (11). In B, total counts m enclosed within profile (such as those in A) of displayed diameter s when divided by its height h (i.e.

normalized to unit height) are proportional to s from 1 to 4 cm. In C, the height of profile h is seen to be approximately proportional to disk diameter d when disks contain same concentration of radioactivity because of poor total resolution of gamma-camera system. Full line was obtained using parallel-holed multichannel collimator and dotted line using pinhole, normalizing at 4 cm point.

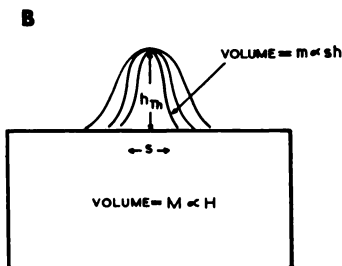
'SQUARE' PROFILES. (MORGAN'S CASE)



THRESHOLD CONDITIONS. ∴ $\frac{m_{Th}}{\sqrt{M}} \propto s$

∴ $\frac{sh_{Th}}{H} = \text{CONSTANT.}$

OUR PROFILES.



$\frac{m_{Th}}{\sqrt{M}} \propto s$

∴ $\frac{h_{Th}}{H} = \text{CONSTANT.}$

FIG. 6. Pictorial representation of visual threshold criteria for square profiles (which gave Figs. 3B) and for gamma-camera profiles (which gave Fig. 3A).

A similar analysis on Morgan's curves shows that the equivalent of $h_{Th}/H^{1/2}$ is an increasing function with decreasing disk size which is a direct result of his "square" profiles, as is shown later.

Figure 6 is a pictorial aid in understanding these relationships. This shows the profile height in counts, superimposed on a background height in counts; i.e., a "count-space" diagram. Figure 6A shows that for a given H and therefore given background counts, the product of the height of the profile h and the width of the profile s is constant for threshold perception. Hence, for perception the smaller the diameter, the bigger the profile height, but also the *smaller its volume* since volume varies as s^2 for a cylindrically shaped count volume. Figure 6B shows the case we found in practice. For a given H it is the *height* of the profile that is constant for threshold detection; the volume m varies as s as explained earlier.

Figure 7 shows a plot of h_{Th}/H as a function of H derived by taking $h_{Th}/H^{1/2} = 1.40$ (Eq. 3) for all values of s and incorporates Figs. 3C, 4 and 5B. Alternatively, this graph can be drawn for each value of s from the graphs of Figs. 3A and 5B.

As is shown, h_{Th}/H is never less than 20% up to a total background count of 10,000. This is the same as the ratio of counting rates (because the camera views the whole field of view for the same time) and therefore compares directly with the typical perception value of 10% for color and photoscan displays and approximately 20% for black-mark displays. It is to be expected that the cathode-ray-tube display should be similar in result to that of black-mark displays since they are very much alike in their presentation. The corresponding values of the threshold fractional counting-rate changes for the three conventional displays previously described are shown marked in Fig. 7.

We are much indebted to a referee of this paper for suggesting the following analysis of the cathode-ray-tube display: Suppose that the observer perceives a difference between the "tumor" and "normal" regions by comparing visually the total counts N_t distributed over the "tumor" region with the counts N_b over a "normal" region of the *same* size and in effect performs a statistical test of the significance of the observed difference.

Let A be the area of the cathode-ray tube and a the area of the "tumor" region.

Then $N_t = m_{Th} + aM/A$

and $N_b = aM/A$

The true mean difference in counts is $m_{Th} = N_t - N_b$, and the standard deviation of the difference is

$$\sigma_{N_t - N_b} = (\sigma^2_{N_t} + \sigma^2_{N_b})^{1/2} = (m_{Th} + 2aM/A)^{1/2} \doteq (2aM/A)^{1/2} \text{ if } m_{Th} \text{ is small compared to } aM/A.$$

The number of standard deviations of difference, n, is given by

$$n = \frac{N_t - N_b}{\sigma_{N_t - N_b}} \doteq \frac{m_{Th}}{(2aM/A)^{1/2}}$$

Now,

$$a = \pi s^2/4$$

Therefore $m_{Th}/M^{1/2} = n(\pi/2A)^{1/2}s$

as we found in practice (see Eq. 1). The constant of proportionality that we found was $k \doteq 0.80$. It is interesting that this corresponds to a value of n of approximately 5. Thus the curve in Fig. 7 for the cathode-ray-tube display, which is the experimentally determined visual threshold, is equivalent to a statistical curve corresponding to a statistical threshold of 5 standard deviations of difference.

To summarize this display section, the following may be observed:

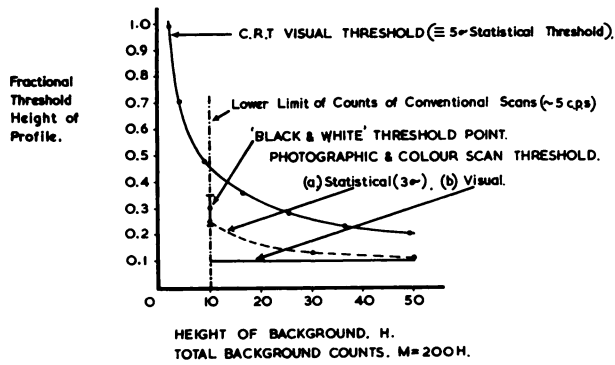


FIG. 7. Variation of fractional threshold counting-rate height with background counting-rate height for all displays.

1. Colored marks on white paper and photographic displays are both capable of detecting 10% changes in counting rate from a lesion of any size within the body provided the background counting rate is itself not changing rapidly around that region. This 10% figure must be regarded as the best that can possibly be done for these displays.

2. Black marks on white paper or cathode-ray-tube displays can detect (at best) 20% changes in counting rate and are subject to the conditions stated above.

3. The important difference that exists between the perception threshold criteria for color and photographic displays on the one hand and cathode-ray-tube displays when used with gamma cameras on the other is that the fractional increase of counting rate producing the perceived profile for the former is independent both of its diameter and the background counting rate; for the cathode-ray-tube display, the same expression is independent of the size of the displayed profile, *but dependent on background counts*; the relationship is a reciprocal square-root law (Fig. 7). In addition, if the fractional increase of *total* counts is considered, then the threshold for the cathode-ray-tube display is dependent on both these quantities as shown in Fig. 3.

4. The visual threshold conditions for the cathode-ray-tube display appear to be identical to a statistical threshold of 5 standard deviations of difference if it can be assumed that the eye examines and compares a similar area of background to the "tumor" area.

PHANTOM EXPERIMENT FOR EVALUATING SCANNER PERFORMANCE

The phantom experiment for evaluating the performance of a scanner attempts to relate the counting-rate profiles obtained either by a conventional scanner or a gamma camera in a given clinical situation to the perception characteristics of the display being used. These characteristics have been investigated in the preceding section, and the results can

be used directly with the results of the phantom experiment described now to provide an estimate of the minimum tumor diameter that can be detected in the chosen clinical situation.

Hollow disks 1 cm thick and 1, 2, 3, 4 and 6 cm in diameter are filled with a known isotope activity and lowered into a water tank (or MIX D tissue-equivalent wax) as shown in Fig. 8. The counting rate obtained for one disk diameter with a particular collimator-counter system is determined when the disk is directly below the collimator; i.e., on its central axis. This is carried out for different depths in the phantom, and the counting rate per unit concentration n_0 is then calculated for that disk at each depth. This experiment is repeated for each disk size, and the values of n_0 are plotted against depth in phantom for each diameter.

Assuming that a clinical lesion approximates a cylinder whose diameter is equal to its thickness, the value of the counting rate due to the lesion is found by summing (from curves drawn of the experimental results) the counting rates n_0 of the superposed incremental disks over the appropriate depth range of the phantom. This procedure is based on the phantom system proposed by MacIntyre, Christie and Tatsuno (12). It is worth pointing out here that from this small series of experimental measurements it is possible to determine the incremental counting rate from shapes approximating spheres or any other shape of circular section. There is no rea-

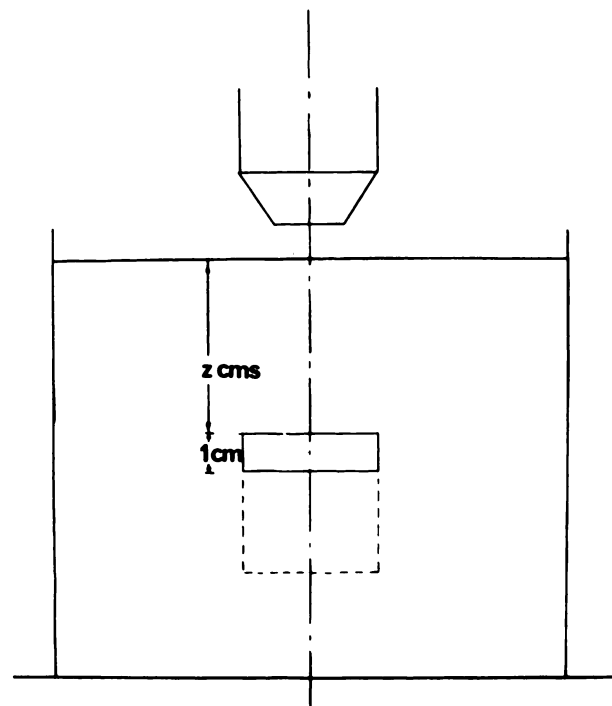


FIG. 8. Diagrammatic representation of phantom experiment.

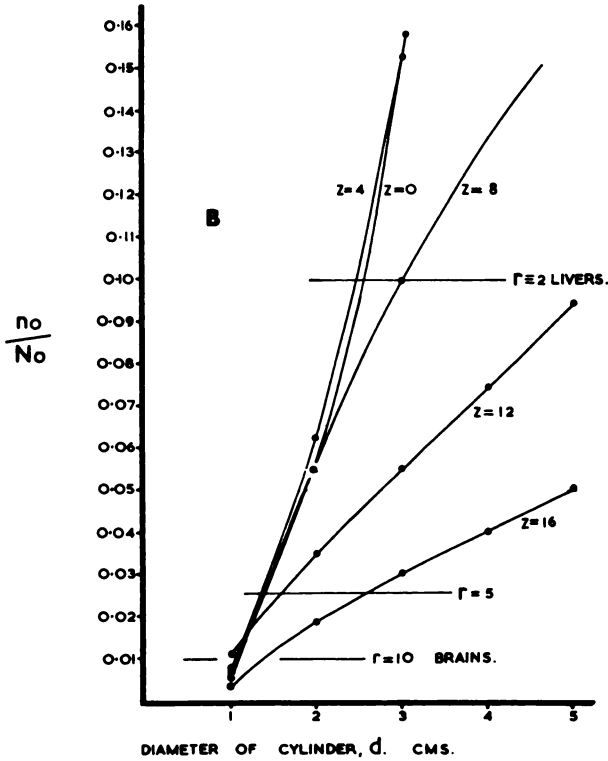
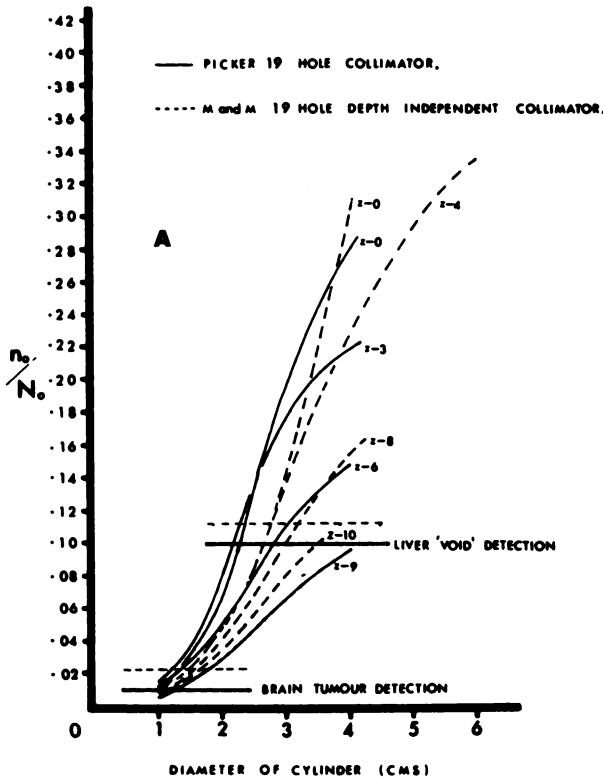


FIG. 9. Plot of n_0/N_0 (see text) against diameter of cylinder (diameter = thickness). Each curve is plotted for one depth in the phantom. In A are full lines for Picker 19-hole collimator with dotted lines for M and M "depth-independent" collimator (14); in B are results from collimator designed for ^{90m}Tc .

son at all why linear shapes should not be measured and used in the same manner.

With the disks removed and the tank filled with the radioactive substance, the counting rate per unit concentration from the tank N_0 is obtained. The size of the tank is chosen to simulate the appropriate part(s) of the body under consideration.

The technique is also applicable to gamma cameras, but additional measurements of the size of the display on the cathode-ray tube for each disk in each position were taken. Also, for the measurements reported here a bidimensional quantitative print-out of the display for each case was obtained, but this is not necessary when the phantom procedure is to be used by other workers.

From these measurements it is possible to forecast the central-axis counting rate (both body background and that due to the tumor) that will be obtained in a given clinical situation. Having previously determined the visual threshold characteristics of the relevant display, an estimate can be made of whether the lesion would be perceived in that clinical situation. Other workers can use the information described in the second section if their display system is similar to one of those used here, or they may prefer to investigate the visual threshold characteristics of their own display system.

The results here are split into two parts for convenience:

1. Conventional moving detectors using either color display or photographic display which have a threshold counting rate change of 10% for perception.

2. Stationary detectors (gamma cameras) together with the perception characteristics of the cathode-ray-tube display.

Moving-detector scanners. In relating the counts obtained in a given clinical situation to the above experiment, we have the following:

$N = N_0 C$, where N is cps from uniform background with a concentration $C \mu\text{C/ml}$, and

$n = n_0 (c - C)$ where n is cps above background due to a cylinder with a concentration $c \mu\text{C/ml}$. For a given collimator and gamma-ray energy, n_0 is a function of depth in phantom and diameter of lesion.

As shown earlier for a color or photographic display, $n_{Th}/N = 0.10$. Thus for threshold perception,

$$\frac{n_{Th}}{N} = \frac{n_0}{N_0} (r - 1) = 0.10 \tag{4}$$

i.e.,
$$\frac{n_0}{N_0} = \frac{0.1}{r - 1}$$

for threshold perception where r is the concentration ratio c/C .

BRAIN. CONCENTRATION RATIO = 10.

LIVER. CONCENTRATION = 2

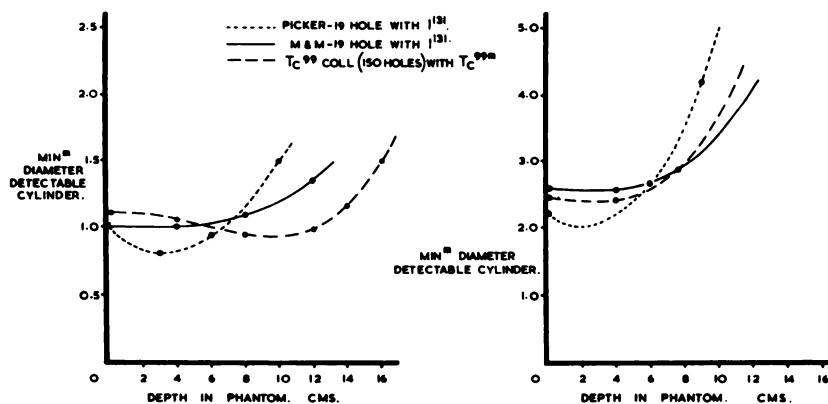


FIG. 10. Performance of a moving-detector scanner using three different detectors with color or photographic display. Plotted here are intersections of curves with horizontal lines in Figs. 9A and B which show over-all performance of scanning system.

Thus all the phantom results (which cover any clinical conditions for any detector system) may be plotted together on one graph in the form n_o/N_o . They have the general appearance shown in Fig. 9A and B. The counters used for these curves are the Picker counter (3-in.-dia crystal) with the 19-hole collimator, the specially designed ^{99m}Tc collimator being used at the Royal Infirmary, Aberdeen (with a 50% resolution diameter of 8 mm at 16 cm in the phantom), and the 19-hole "depth independent" collimator (14) for higher-energy gamma emitters, both with a 3½-in.-diameter crystal. Other collimators were investigated but are not included here.

To see how these collimators would perform for a brain scan, assuming a tumor-to-normal brain tissue-concentration ratio of 10 and for a liver scan in which the concentration ratio is effectively 2 (13), we draw lines across this graph with height of $0.1/(r-1)$, as shown in Fig. 9 and read off the intersections with the curves. These intersections are shown in Fig. 10 and represent the minimum sizes of cylindrical tumors (diameter = thickness) which produce a counting-rate profile with the counter and collimator used which in turn the display can render perceptible to the eye. It must be borne in mind that this is the best possible result obtainable, smaller tumors producing counting-rate changes below the threshold of perception for the display system used.

Such estimations are considered to be consistent with the type of result expected for each particular collimator; e.g., the "M and M" collimator (4) shows relatively more depth independence when compared with the 19-hole Picker collimator which has a superior performance up to about 6 cm depth but has a more rapid fall-off afterwards. Also it is known from experience and from the literature that tumors less than 1 cm in size are not usually detected

by brain scanning; thus the result is in agreement with the predictions of Figs. 9 and 10.

The phantom experiment can be used to redesign counter systems. For example, for our ^{99m}Tc collimator, it is thought that the 50% resolution diameter of 8 mm may be too good because the response suddenly improves in the region of the radiation focus in the phantom. An increase of the resolution to 1.0 cm may improve the whole curve of Fig. 10 while making the response more uniform with depth.

The effect of laboratory background is also shown by the dotted lines in Fig. 9. The laboratory background B modifies Eq. 4 to

$$\frac{n_o}{N_o} = \frac{0.1}{(r-1)} \times \left(1 + \frac{B}{N_o C} \right)$$

so that if $B \leq N_o C$, a negligible correction factor is introduced; i.e., if the laboratory background is considerably less than the counting rate due to the body and organ background, the correction is negligible as one would expect. In both the brain and liver cases shown, the laboratory background does not significantly increase the lesion diameter which is detectable.

In the very preliminary report of this phantom procedure (8) the method of plotting the results was not as elegant as that described here because the procedure was longer and more lines had to be plotted at that time. (Families of counting-rate curves had to be plotted for each different concentration ratio and the horizontal line for display perception had to be drawn at different heights for different body background counting rates.)

Stationary-detector scanners. The phantom procedure can be used with a stationary-detector scanner both with and without a multichannel analyzer.

Using a multichannel analyzer. Having determined

the characteristics of the cathode-ray-tube display using a multichannel analyzer, it seemed reasonable to use these results to estimate the minimum cylinder size that can be detected. This was done using the following identities:

$$M = N_0 Ct \quad \text{where } M \text{ and } C \text{ are defined as previously and } t \text{ is the integration time in seconds}$$

$$= 200 H, \text{ the picture being contained in 200 channels of the multichannel analyzer.}$$

$$m = n_0 (c - C)t$$

and $h_{Th}/H^{1/2} = 1.40$ for threshold perception (Eq. 3). Now, we define $W = h/m$ which is measured in the phantom experiments using a multichannel analyzer. W is a descriptive term for the counting-rate profiles presented by the camera to its display.

Combining all the above equations:

$$Wm_{Th} = h_{Th} = 1.40 H^{1/2} = 0.10 M^{1/2}$$

i.e.,

$$m_{Th} W/M^{1/2} = 0.10$$

$$\text{Now} \quad \frac{m}{M^{1/2}} = \frac{n_0}{N_0^{1/2}} (r - 1) (Ct)^{1/2} \quad (5)$$

$$\therefore \frac{n_0}{N_0^{1/2}} W = \frac{0.10}{(r - 1) (Ct)^{1/2}} \quad (6)$$

for threshold perception.

Thus all the phantom results can be plotted on one graph as was possible in the case of moving detectors. The ordinate now is $n_0 W/N_0^{1/2}$ (which is proportional to $h/H^{1/2}$) as shown in Fig. 11 for a gamma camera using a parallel-hole multichannel collimator (11). The curves obtained using a pinhole are not shown.

Equation 6 shows that the probability of detection increases with concentration ratio, background concentration and time of exposure. This equation sepa-

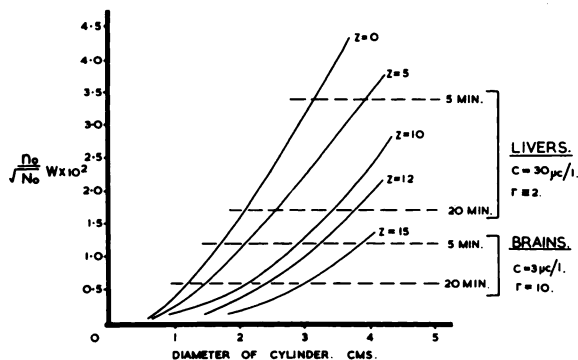


FIG. 11. Plot of $n_0 W/N_0^{1/2}$ (see text) measured with gamma camera using multichannel collimator as function of cylinder diameter at different depths in phantom. Two sets of clinical conditions using ^{131}I are postulated, one typical of liver scanning, other of brain scanning for two exposure times shown.

rates out the three variables of scanning: the detector performance (left-hand side), the clinical conditions (right-hand side) and the display properties (right-hand side), as does Eq. 4.

Horizontal lines of height equal to the value of the right-hand side of Eq. 6 are drawn on Fig. 11, for typical cases of brain and liver scans where the clinical conditions are stated in the figure. The resulting minimum diameter of tumor that can just be detected and its variation with depth in phantom for an exposure time of 5 and 20 min are shown in Fig. 12.

Without a multichannel analyzer. For those workers who are not in a position to use a bidimensional multichannel analyzer in conjunction with their gamma camera, the following very similar procedure can be used: The basic phantom experiment is carried out as previously explained with total counts measured for each disk in each position using a scaler and a measurement of the displayed diameter s for each case. The equivalent of Eq. 6 is:

$$\frac{1}{s} \frac{n_0}{N_0^{1/2}} = \frac{0.80}{(r - 1) (Ct)^{1/2}}$$

for threshold perception obtained from Fig. 4 and Eq. 5).

Again, one graph can be drawn [$(1/s) (n_0/N_0^{1/2})$ as a function of cylinder diameter at each depth] and horizontal lines of detection used to determine the threshold diameters of cylinders.

These two methods for stationary detectors agree well when used independently in our experiment (within about 0.10 cm throughout the range of depth in phantom and the diameters of cylinders). The second method is probably preferable because fewer steps are involved. However, we have shown that it is possible to use profile heights throughout so that the cathode-ray-tube display can be compared with the conventional displays at any stage of the argument.

From Fig. 12 one sees that the pinhole does surprisingly well when compared with the parallel-hole collimator, but the experiment was biased in its favor because the surface of the phantom was at a distance from the pinhole which was more compatible with thyroid scans than liver and brain scans. However, its greater depth dependence is apparent, as is also the much greater depth dependence of the camera with the multichannel collimator than the focusing collimators of moving-detector systems. This disadvantage of the gamma camera is unlikely to be overcome by using multichannel parallel-hole collimators.

The results shown in Fig. 12 illustrate the value of the phantom procedure because it predicts sizes

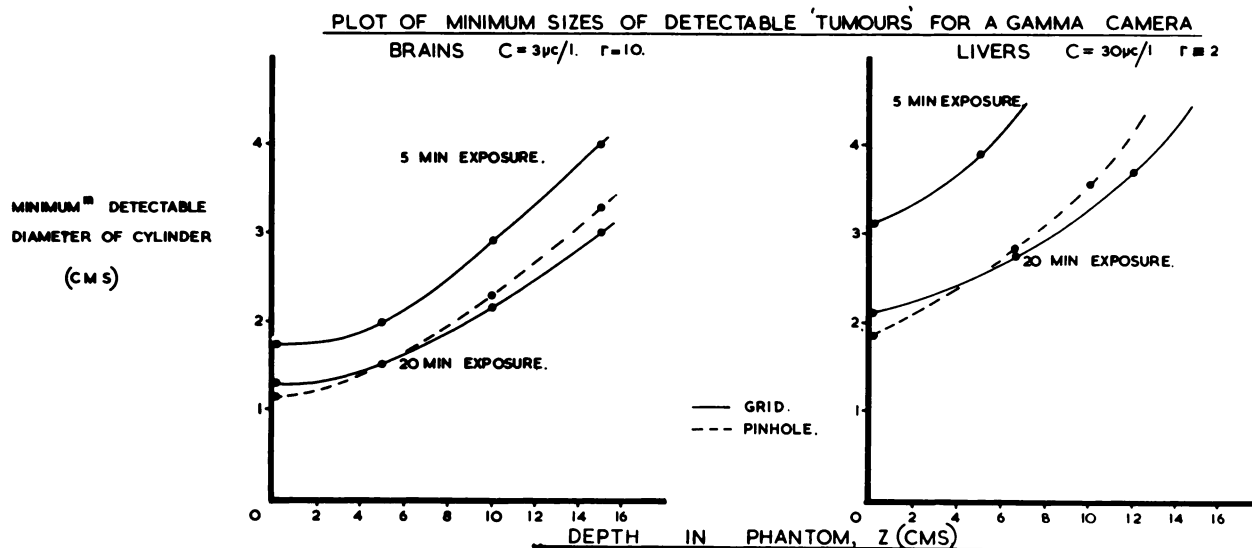


FIG. 12. Performance of gamma camera using both pinhole and multichannel parallel-holed collimators (grid). Plotted are intersections of curves with horizontal lines in Fig. 11.

of minimum detectable tumors which agree well with one's clinical experience and reports in the literature of gamma-camera performance. Figures 10 and 12 also illustrate the relationship between the performance of a gamma camera and moving-detector scanners for tumors near the surface of the phantom when their performance is very similar.

COMMENTS AND DISCUSSION

Considering Eq. 4, it is seen that the term $1/(r-1)$ decreases slowly with increasing r for r greater than about 10 so that very significant increases in the concentration ratio r are needed if tumors much less than about 1 cm are to be seen (see Fig. 9) with the counters used here which can be regarded as being typical ones.

This effect also applies to gamma cameras (Eq. 6), because the term $1/(r-1)(Ct)^{1/2}$ decreases slowly for $(r-1)(Ct)^{1/2}$ greater than about 10; the value of t at which this occurs is defined here as t_{10} . For $C = 30\mu\text{C}/\text{l}$ ^{131}I , $r = 2$ as in a liver scan and $t_{10} = 50$ min, and for $C = 3\mu\text{C}/\text{l}$ ^{131}I , $r = 10$ as in a brain scan and $t_{10} = 8$ min. (If r is reduced to 6 in the last example, $t_{10} = 20$ min.) It would seem from this that longer exposure times than those normally used may result in some gain, but it is apparent that to detect much smaller lesions either better display systems must be provided or the performance curves (similar to those of Fig. 9) must be considerably improved in the smaller diameter regions.

It might be convincingly argued that although any 10% increase in counting rate will be perceived from the color and photographic displays, this might not be statistically significant for a given scan because

it might be an artifact. Other workers (3,5) use the criterion of at least 3 standard deviations (σ) of difference (3) between the suspected and normal areas as a necessary and sufficient condition of detectability,

$$\frac{n'_a - n_a}{(n'_a + n_a)^{1/2}} t^{1/2} \geq 3$$

where n'_a is the counting rate from the square under suspicion, n_a is the counting rate from the normal square and t is the time to scan each square.

It has been shown (15) that for the typical size square used, the statistical limit is somewhere between 2σ and 3σ because a 2σ difference is likely to occur, statistically, whereas there is only an 8% chance for a 3σ change (i.e., there is 92% confidence in change being genuine) when one uses a grid of about 30 squares on a lateral brain scan.

For example, in brain scanning using ^{131}I human serum albumin with typical scanning conditions (couch speed = 0.2 cm/sec, line spacing = $\frac{1}{2}$ cm, typical $n_a = 15$ cps), we have for a typical square (2.5×2.5 cm) $t = 62.5$ sec so that $n'_a = 17$ cps. Hence $n/N = 0.13$; i.e., a value of 13% for the 3σ criterion, rather than the threshold of 10% as determined in this work. For the higher counting rates (50 cps) obtained from $^{99\text{m}}\text{Tc}$, $n/N = 1.10$; i.e., 10% in agreement with our findings. In the first example, if a black and white display or a cathode-ray-tube display had been used, the 13% increase in counting rate *would not have been perceived visually* although it was a very significant increase in counting rate. The 10% threshold of the color and photographic displays as perceived by the eye can be considered as refining the rigid limit of 3σ because the latter is a fairly arbitrary threshold perception criterion, although a rigid statistical one. Thus we regard 3σ as an overestimate of the necessary cri-

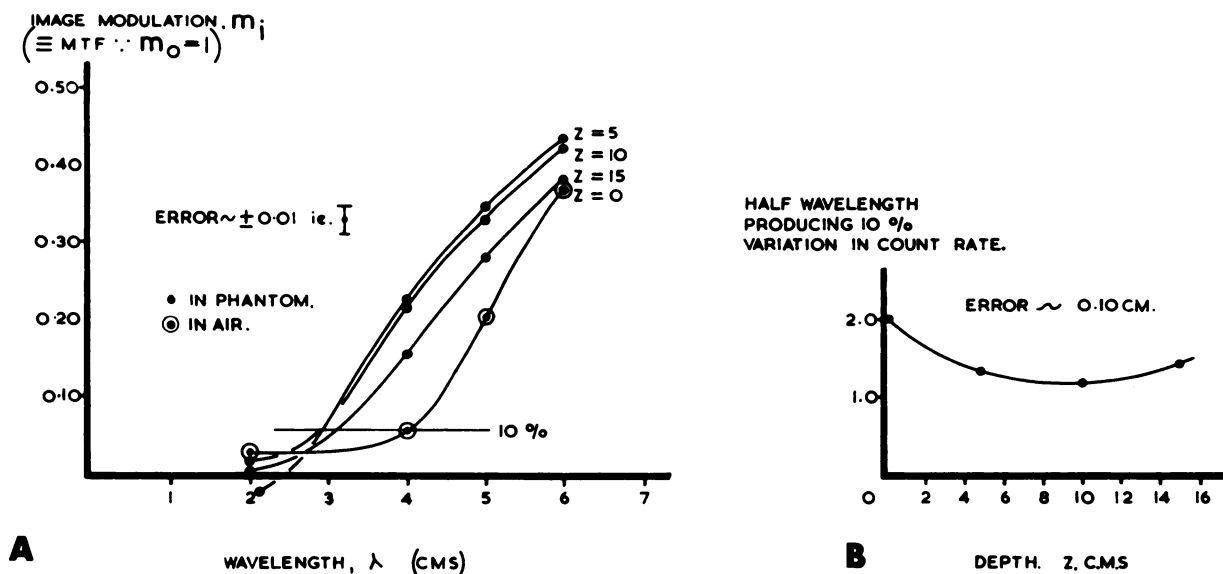


FIG. 13. A shows variation of modulation transfer function with wavelength for different depths in phantom. Image modulation from sinusoidal sources of ^{132}I of unit modulation has been measured

with detector using M and M collimator. B shows variation of half-wave length which gives rise to 10% variation in counting rate (image modulation 5%) with depth.

terion for perception when using a display capable of showing less than this: in Fig. 7, the 3σ statistical criterion for perception is drawn to indicate the degree of overestimation.

In addition to the visual perception characteristics of the eye, the analysis of the display described here takes into account both the *statistical nature of the background* (provided an area much larger than the area of the lesion is scanned) and the *area of the increased counting rate* in its "sea" of background.

When this "sea" of counting rate is constant over the area of interest, the criteria mentioned previously are sufficient for the perception of a lesion. However, when the "sea" has a counting-rate gradient of the order of 10% over the area of interest (approximately the "resolution distance" for small lesions) the visual processes involved are more complex, resulting in the visual threshold being raised toward the statistical criterion of 3σ .

Even in a constant background scan, the 3σ criterion departs materially from the 10% figure we have obtained, only when the background counting rate is low (about 10 cps). Thus, at high counting rates there is little difference in the two thresholds. It is interesting to note that the adoption of a 3σ criterion for low counting rates rather than the 10% figure used in this paper only makes a difference of approximately 20% in the minimum diameter of the perceptible lesion for small diameters of lesion.

An attempt was made to relate the modulation transfer function (MTF) approach to the method described here. The MTF has been proposed by

Beck (6) and used by Craddock, *et al* (16).

Using a source modulation of unity, the "image modulation" was measured both in air and in MIX D phantom as a function of depth using the "depth-independent" collimator (14). Since only photopeak disintegrations were recorded, scattered radiation was virtually eliminated (only primary radiation is recorded) so that any differences resulting from the use of the two media were attributed to the modification of the isocount lines of the counter by the phantom (attenuation effects).

A plot of the "image modulation" (\equiv MTF since object modulation is 1) with depth in phantom is shown in Fig. 13A. The curve for the surface of the phantom is the same as that in air at the same distance. As an interesting experiment, the half-wave length (related to disk diameter) giving rise to a 10% variation of counting rate was plotted against depth (Fig. 13B) as an attempt to correlate the phantom experiment described in this study with the MTF approach. However, it is uncertain to what clinical conditions (e.g., concentration ratio) this is analogous, and further analysis is necessary before the two approaches can be properly related.

The MTF of an instrument indicates how well an activity distribution of a particular spatial frequency is maintained right through the detecting system to the display and, as it stands, does not make an estimate of whether such a distribution is perceived. It appears to us that MTF measurements of display systems, the eye and some form of threshold perception experiment is required.

To summarize the phantom experiment in this paper, the following observations can be made:

1. The results of the phantom procedure for both the moving and stationary detectors can be plotted in such a way that any change in clinical conditions can be accounted for by varying the height of only the horizontal line so that it is not necessary to replot the curves for each case, as was necessary in a preliminary communication of this procedure (8).

2. The inherent degradation in the response of a gamma camera with depth in tissue with either multi-channel collimator or pinhole is well brought out in the figures. It is difficult to see how this can be overcome.

3. The estimated sizes of minimum diameters of tumors that can be detected are consistent with clinical work and with the literature.

4. The phantom experiment can be used to redesign counter systems.

In conclusion, a simple phantom experiment is described which, together with a criterion for threshold visual detectability for the display being used, yields the estimate of the minimum tumor size that can be detected in a known clinical condition.

We hope that the flexibility of the method will appeal to other workers so that, in addition to comparing collimators by means of figures of merit, line-spread function and modulation transfer function, they may also be compared in this way which we believe is practical and clinically more meaningful.

REFERENCES

1. MALLARD, J. R.: Medical radioisotope scanning. *Phys. Med. Biol.* 10:309, 1965.
2. MALLARD, J. R.: Medical radioisotope visualisation (A review of "scanning"). *Inter. J. of Appl. Radiation Isotopes* 17:205, 1966.
3. DEWEY, W. C., AND SINCLAIR, W. K.: Criteria for evaluating collimators used in in-vivo distribution studies with radioisotopes. *Inter. J. Appl. Radiation Isotopes* 10:1, 1961.
4. BECK, R. N.: A theoretical evaluation of brain scanning systems. *J. Nucl. Med.* 2:314, 1961.
5. MATTHEWS, C. M. E.: Comparison of coincidence counting and focusing collimators with various isotopes in brain tumour detection. *Brit. J. Radiol.* 37:531, 1964.
6. BECK, R. N.: A theory of radioisotope scanning systems. In *Medical radioisotope scanning* (IAEA, Vienna), 1964, p. 35.
7. MALLARD, J. R. AND PEACHEY, C. J.: A scanning machine for presenting pictorially and quantitatively the distribution of radioisotopes in-vivo. *Proc. 3rd inter. conf. med. electronics, I.E.E.*, London, 1960, p. 511.
8. MALLARD, J. R., DUGGAN, M. H., MYERS, M. J. AND WILKS, R. J.: in *Medical radioisotope scanning*, IAEA, Vienna, 1964, p. 423.
9. LAUGHLIN, J. S., KENNY, P. J., COREY, K. R., GREENBERG, E. AND WEBER, D. A.: Localization and total body high-energy gamma ray studies in cancer patients. In *Medical radioisotope scanning*, IAEA, Vienna, 1964, p. 253.
10. MORGAN, R. H.: Threshold visual perception and its relationship to photon fluctuation and sine wave response. *Am. J. Roentgenol Radium Therapy Nucl. Med.* 93:982, 1965.
11. WILKS, R. J. AND MALLARD, J. R.: A small gamma camera—improvements in the resolution, a setting-up procedure and a digital print-out. *Inter. J. Appl. Radiation Isotopes* 17:113, 1966.
12. MACINTYRE, W. J., CHRISTIE, J. H., AND TATSURO, I.: The evaluation of straight bore, tapered and focusing collimators as a function of gamma energy. In *Medical radioisotope scanning*, IAEA, Vienna, 1964, p. 153.
13. BENDER, M. A.: in *Medical radioisotope scanning*, IAEA, Vienna, 1959, p. 251.
14. MYERS, M. J. AND MALLARD, J. R.: Some long-focusing "depth independent" collimators for in-vivo radioisotope scanning. *Inter. J. Appl. Radiation Isotopes* 15:725, 1964.
15. HAYBITTLE, J. L.: The quantitative analysis of cerebral scintiscans. *Phys. Med. Biol.* 11:474, 1966.
16. CRADDOCK, T. D., FEDORUK, S. O., AND REID, W. B.: A new method of assessing the performance of scintillation cameras and scanners. *Phys. Med. Biol.* 11:423, 1966.